Dalton Transactions

Accepted Manuscript

ROYAL SOCIETY OF CHEMISTRY

www.rsc.org/dalton

Dalton Trans.

ARTICLE

Six-coordinate Ferric Porphyrins Containing Bidentate *N*-*t*-Butyl-*N*-nitrosohydroxylaminato Ligands: Structure, Magnetism, IR spectroelectrochemisty, and Reactivity

Received 00th January 20xx,
Accepted 00th January 20xx

DOI: 10.1039/x0xx00000x

www.rsc.org/

Nan Xu,*[a,b] Jonathan H. Christian,[c] Naresh S. Dalal,*[c] Erwin G. Abucayon,[a] Colin Lingafelt,[b] Douglas R. Powell,[a] and George B. Richter-Addo*[a]

Abstract: NONOates (diazeniumdiolates) containing the $[X\{N_2O_2\}]^-$ functional group are frequently employed as nitric oxide (NO) donors in biology, and some NONOates have been shown to bind to metalloenzymes. We report the preparation, crystal structures, detailed magnetic behavior, redox properties, and reactivities of the first isolable alkyl *C*-NONOate complexes of heme models, namely (OEP)Fe(η^2-ON(*t*-Bu)NO) (**1**) and (TPP)Fe(η^2-ON(*t*-Bu)NO) (**2**) (OEP = octaethylporphyrinato dianion, TPP = tetraphenylporphyrinato dianion). The compounds display the unusual NONOate *O,O*-bidentate binding mode for porphyrins, resulting in significant apical Fe displacements (+0.60 Å for **1**, and +0.69 Å for **2**) towards the axial ligands. Magnetic susceptibility and magnetization measurements made from 1.8–300 K at magnetic fields from 0.02 to 5T, yielded magnetic moments of 5. 976 and 5.974 Bohr magnetons for **1** and **2**, respectively, clearly identifying them as high-spin ($S = {}^5/_2$) ferric compounds. Variable-frequency (9.4 GHz and 34.5 GHz) EPR measurements, coupled with computer simulations, confirmed the magnetization results and yielded more precise values for the spin Hamiltonian parameters : g_{avg} = 2.00 ± 0.03, $|D|$ = 3.89 ± 0.09 cm^{-1}, and E/D = 0.07 ± 0.01 for both compounds, where D and E are the axial and rhombic zero-field splittings. IR spectroelectrochemistry studies reveal that the first oxidations of these compounds occur at the porphyrin macrocycle and not at the Fe-NONOate moieties. Reactions of **1** and **2** with a histidine mimic (1-methylimidazole) generate RNO and NO, both of which may bind to the metal center if sterics allow, as shown by a comparative study with the Cupferron complex (T(*p*-OMe)PP)Fe(η^2-ON(Ph)NO). Protonation of **1** and **2** yields N_2O as a gaseous product, presumably from the initial generation of HNO that dimerizes to the observed N_2O product.

gfgf

1 Introduction

The NONOate (diazeniumdiolate) functional group formally contains two NO moieties linked to an organic fragment X as sketched in Figure 1. The most widely-known NONOates contain carbon-bound (*C*-NONOates) and nitrogen-bound (*N*-NONOates) organic fragments, although several NONOates containing *S*-bound and *O*-bound fragments are also known.[1]

C-NONOates have attracted a lot of attention from the viewpoint of their coordination chemistry. For example, the Cupferron anion (i.e., $[Ph\{N_2O_2\}]^-$) binds to several metal ions, and has been widely used historically as an analytical reagent for the colorimetric detection of Fe and Cu.[2] However, there is also biological interest in the chemistry of *C*-NONOate compounds due to the fact that the *C*-NONOate functional group is present in several natural products including the antitumor antibiotic alanosine isolated from *Streptomyces alanosinicus*[3, 4] and the free radical scavenger poecillanosine isolated from the marine sponge *Poecillastra* spec. aff. *tenuilaminaris* (Figure 1),[5] and several

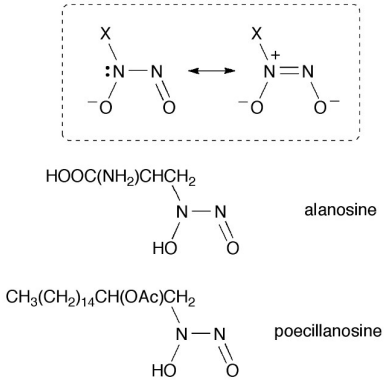

Fig. 1 *Top*: Sketch of the NONOate functional group showing the common resonance forms. *Bottom:* Chemical structures of the NONOate-containing natural products alanosine and poecillanosine.

[a] Department of Chemistry and Biochemistry, University of Oklahoma, 101 Stephenson Parkway, Norman, OK 73019. Email: grichteraddo@ou.edu.
[b] Division of Mathematics and Natural Sciences, Penn State Altoona, 3000 Ivyside Park, Altoona, PA 16601. Email: nxx103@psu.edu.
[c] Department of Chemistry and Biochemistry, Florida State University, 95 Chieftan Way, Tallahassee, FL 32306. Email: dalal@chem.fsu.edu

† Footnotes relating to the title and/or authors should appear here.
Electronic Supplementary Information (ESI) available: [details of any supplementary information available should be included here]. See DOI: 10.1039/x0xx00000x

others such as dopastin and fragin.[1] *C*-NONOates such as Cupferron and the related *N*-NONOates are frequently employed as NO donors in physiological media.[6]

NONOates bind to metals in coordination compounds almost exclusively via the bidentate *O,O*-binding mode.[2] The only structurally characterized exception of an observed monodentate *O*-binding mode is that of a Cu complex containing the ($[Et_2N\{N_2O_2\}]^-$) ligand.[7]

Given the biological importance of *C*-NONOates, we were interested in determining what kind of interactions would be present if *C*-NONOates encounter heme. We note that Cupferron is a good substrate for horseradish peroxidase (releasing PhNO and NO),[8] and that a direct binding of an *N*-NONOate to the metal center of cobalamin has been shown to precede the release of NO.[9] Interestingly, a related direct binding of the natural product Dopastin via its NONOate functional group to the di-Cu active site of mushroom tyrosinase has been proposed to precede the observed inhibition of this enzyme.[10]

We now report the preparation, crystal structures, detailed magnetic behavior, redox properties, and reactivities of two alkyl *C*-NONOate complexes of heme models. Combined with our initial report on a Cupferron complex,[11] these remain the only isolable NONOate complexes of heme models reported to date.

2 Experimental

2.1 Synthesis

The reactions were performed anaerobically using nitrogen as the inert gas. Standard Schlenk glassware and an inert atmosphere glove box were utilized for the syntheses. Solvents were distilled under nitrogen from appropriate drying agents or collected under nitrogen from a Pure Solv 400-5-MD Solvent Purification System (Innovative Technology). *N*-*t*-butyl-*N*-nitrosohydroxylamine (HON(*t*-Bu)NO) was prepared by literature methods.[12] The Cupferron salt Ag[ON(Ph)NO] was prepared as described previously.[13] FT-IR spectra for compound characterization were recorded on a Bio-Rad FTS 155 spectrometer. Elemental analyses were performed by Atlantic Microlab, Inc., Norcross, GA.

Preparation of (OEP)Fe(η^2-ON(*t*-Bu)NO) (1). To a CH_2Cl_2 (10 mL) solution of $[(OEP)Fe]_2(\mu$-O) (25 mg, 0.021 mmol) under an atmosphere of nitrogen was added a CH_2Cl_2 solution (2.5 mL) of excess *N*-*t*-butyl-*N*-nitrosohydroxylamine (68 mg, 0.58 mmol, ~28x excess). The solution was stirred for 1 h during which time the color changed gradually from brown to purple-red. The solvent was removed under vacuum. Hexane (~5 mL) was added to the residue, and the mixture stirred for ~ 1 min and left to stand for 5-10 min. The light red supernatant was discarded and the remaining dark purple solid dried in vacuo overnight to give (OEP)Fe(η^2-ON(*t*-Bu)NO) (**1**) (16 mg, 0.022 mmol, 55% isolated yield). Anal. Calcd for $C_{40}H_{53}N_6O_2Fe.0.055CH_2Cl_2$ (MW 710.40): C: 67.72; H, 7.53; N, 11.83; Cl, 0.55. Found: C, 67.73; H, 7.58; N, 11.73; Cl, 0.53. IR (KBr) spectroscopy revealed a new peak at 1166 cm^{-1} assigned to the ligand. X-ray quality crystals were obtained by a slow evaporation of a CH_2Cl_2/hexane (2:1) solution of the complex under nitrogen. Residual CH_2Cl_2 was present in the sample sent for elemental analysis (as judged by Cl analysis), but it was not detectable by X-ray diffraction.

Preparation of (TPP)Fe(η^2-ON(*t*-Bu)NO) (2). The tetraphenylporphyrin derivative of **1** above, namely (TPP)Fe(η^2-ON(*t*-Bu)NO) (**2**), was obtained similarly in 68% isolated yield. Anal. Calcd for $C_{48}H_{37}N_6O_2Fe.0.74CH_2Cl_2$ (MW 933.44): C, 68.99; H, 4.57; N, 9.90; Cl, 6.18. Found: C, 69.23; H, 4.86; N, 9.61; Cl, 6.25. IR (KBr, cm^{-1}): 1163 (sh) and 961 (m) cm^{-1} assigned to the ONNO moiety. X-ray quality crystals were obtained by a slow evaporation of a CH_2Cl_2/cyclohexane (2:1) solution of the complex under nitrogen. Fractional CH_2Cl_2 was present in the sample sent for elemental analysis (as judged by Cl analysis), but it was present in full occupancy in the structure obtained by X-ray diffraction.

Preparation of (OEP)Fe(η^2-ON(Ph)NO) (3). The synthesis was performed under reduced laboratory lighting to minimize the light-induced decomposition of the product. To a Schlenk tube charged with (OEP)FeCl (23.1 mg, 0.04 mmol) in CH_2Cl_2 (10 mL) was added an excess of freshly prepared Ag[ON(Ph)NO] (22.3 mg, 0.09 mmol). The mixture was stirred for 15 min during which time the color changed from brown-red to bright red-orange. The solution was then filtered via cannula and the solvent removed in vacuo. The dark residue was washed with hexane and dried in vacuo to give (OEP)Fe(η^2-ON(Ph)NO) (**3**) (15.7 mg, 59% yield). IR (KBr, cm^{-1}): 1340 (m), 1283 (s), 940 (m) cm^{-1}, assigned to $\upsilon_{N=N}$, υ_{NO} and δ_{ONNO}, respectively.

Preparation of (T(*p*-OMe)PP)Fe(η^2-ON(Ph)NO) (4).[11] The (T(*p*-OMe)PP) derivative of **3** above was obtained similarly in 63% yield (46.0 mg) from the reaction of (T(*p*-OMe)PP)FeCl (65.0 mg, 0.08 mmol) in CH_2Cl_2 (10 mL) and excess of freshly prepared Ag[ON(Ph)NO)] (64.3 mg, 0.26 mmol) under reduced laboratory lighting. IR (KBr, cm^{-1}): δ_{ONNO} = 937 cm^{-1}. The IR frequencies due to N=N and N=O vibrations were not detected due to the intense porphyrin ring signals in the region where those peaks are normally expected.

Reactions of the (por)Fe(η^2-ON(R)NO) Complexes (por = OEP, T(*p*-OMe)PP; R = *t*-Bu, Ph) with 1-MeIm. The following reactions performed under reduced laboratory lighting are representative.

(i) To a $CDCl_3$ (3 mL) solution of compound **1** (16 mg, 0.013 mmol) was added excess 1-MeIm (28.2 mg, 0.34 mmol). The reaction mixture was stirred at room temperature for 1 hr during which time the color gradually changed from purple to red-purple. The solvent and volatiles were transferred by vacuum to a separate flask. The remaining solid in the reaction flask was washed with hexane and dried in vacuo to give a mixture of the known (OEP)Fe(NO) (υ_{NO} 1672 cm^{-1}) compound[14] and unreacted **1** as judged by IR spectroscopy. A ^{1}H NMR spectroscopic analysis of the trapped volatiles revealed the formation of *t*-BuNO [δ ppm: 1.6 (s, (*t*-BuNO)$_2$ dimer) and 1.2 (s, *t*-BuNO monomer)][15] as the primary byproduct of the reaction in ~50% unoptimized yield based on **1**.

(ii) To a CH_2Cl_2 (5 mL) solution of (T(*p*-OMe)PP)Fe(η^2-ON(Ph)NO) (**4**; 20.0 mg, 0.02 mmol) was added excess 1-MeIm, and the reaction mixture stirred for ~1 h at –45 °C during which time the color changed from bright red-orange to red-purple. The solvent was removed in vacuo and the residue was washed with hexane and the product dried in vacuo overnight. Crystallization of the residue from the slow evaporation of its CH_2Cl_2/hexane (1:1) solution gave a mixture (~9.0 mg) of the crystalline products (T(*p*-

OMe)PP)Fe(NO) (23% yield; υ_{NO} 1670 cm^{-1})[14] and (T(*p*-OMe)PP)Fe(PhNO)(1-MeIm) (23% yield; υ_{MeIm} 1539 (m), and υ_{NO} 1346 cm^{-1}) in a 1:1 ratio.

The corresponding reaction of (OEP)Fe(η^2-ON(Ph)NO) with excess 1-MeIm similarly gave a 1:1 mixture of (OEP)Fe(NO) (υ_{NO} 1672 cm^{-1}) and (OEP)Fe(PhNO)(1-MeIm) (υ_{MeIm} 1523 (m), and υ_{NO} 1337 cm^{-1})[16] as products in ~21% yield for each product.

Reactions of the (por)Fe(η^2-ON(*t*-Bu)NO) Complexes (por = OEP, TPP) with nitric oxide. Solutions of the (por)Fe(η^2-ON(*t*-Bu)NO) (por: OEP, **1**; TPP, **2**) complexes in CH_2Cl_2 (3 mL) were exposed to NO gas (via bubbling of the gas through the solutions) for 5 min during which time the color of the solutions changed from purple to bright red-purple. The unreacted NO gas in the headspace was then replaced by sparging with N_2 gas for ~5 min. The IR spectrum of the product solution from the reaction of **1** with NO in CH_2Cl_2 displayed a new strong υ_{NO} band at 1883 cm^{-1} ($\upsilon_{^{15}NO}$ =1848 cm^{-1}) assigned to the six-coordinate (OEP)Fe(NO)(η^1-ON(*t*-Bu)NO). The IR spectrum of the product of the reaction of **2** with NO yielded a strong υ_{NO} band at 1888 cm^{-1} ($\upsilon_{^{15}NO}$ =1851 cm^{-1}) assigned to the six-coordinate (TPP)Fe(NO)(η^1-ON(*t*-Bu)NO). Attempted crystallization of the OEP adduct led to the formation of the known five coordinate (OEP)Fe(NO) compound identified by IR spectroscopy and by X-ray crystallography.

Protonation of the (por)Fe(η^2-ON(R)NO) Complexes. The following reactions performed under reduced laboratory lighting are representative.

(i) (TPP)Fe(η^2-ON(*t*-Bu)NO) (**2**): Triflic acid (20 μL, 0.2 mmol) was added dropwise to a $CDCl_3$ (3.0 mL) solution of **2** (13.1 mg, 0.02 mmol) at room temperature. The bright red-purple solution immediately changed to an orange-black color. The reaction mixture was stirred for 1 h in a sealed Schlenk tube. The headspace gases were then vacuum transferred into a gas IR cell. The gas phase IR spectrum revealed bands at 2237/2212 and 1276/1261 cm^{-1} assigned to $\nu_{(antisym)}$ and $\nu_{(sym)}$ of N_2O, respectively.[17]

The remaining reaction solution was vacuum transferred to another flask for ^{1}H NMR spectroscopic analysis. ^{1}H NMR ($CDCl_3$, 253 K, 400 MHz): δ 7.27 (s, $CDCl_3$), 5.32 (s, CH_2Cl_2), 2.21 (s, acetone), 1.75 (s, H_2O), 1.59 (s, (*t*-BuNO)$_2$ dimer) and 1.27 (s, *t*-BuNO monomer),[15] 1.22 (s, unassigned) and 0.06 (s, silicone grease impurity).[18] The solid residue was dried in vacuo and crystallized from the slow evaporation of a CH_2Cl_2-hexane solution of this residue. The resulting crystals were identified from an X-ray structural analysis as the known five coordinate complex (TPP)Fe(OSO_2CF_3).[19]

(ii) (T(*p*-OMe)PP)Fe(η^2-ON(Ph)NO) (**4**): Triflic acid (20 μL, 0.2 mmol) was added dropwise to a CH_2Cl_2 (10.0 mL) solution of **4** (18.2 mg, 0.02 mmol) at room temperature. The bright red-purple solution immediately changed to a dark orange color. The reaction mixture was stirred for 12 h in a sealed Schenk tube, and the headspace gases were then vacuum transferred into a gas IR cell. The gas phase IR spectrum revealed the formation of N_2O.[17] The solvent was then removed from the residual mixture in the Schlenk tube in vacuo. Diethyl ether was added to the oily residue, and the mixture was stirred overnight and then left to stand for several minutes to allow the resulting solid particles to separate. The solvent was discarded and the solid product was dried in vacuo. The IR spectrum of the solid product showed a peak at 1347 (sh) cm^{-1} assigned to an Fe-bound PhNO ligand.

Chemical oxidation of (TPP)Fe(η^2-ON(*t*-Bu)NO). To a $CDCl_3$ (2.5 mL) solution of (TPP)Fe(η^2-ON(*t*-Bu)NO) (5 mg, 0.01 mmol) under reduced laboratory lighting was added $AgBF_4$ (1.5 mg, 0.01 mmol). The reaction mixture was stirred for 15 min during which time the color of the solution changed from purple-red to a bright red. IR spectral analysis of the product solution under N_2 showed the formation of a new band at 1293 cm^{-1} indicative of a TPP-type π-radical cation product.[20]

2.2 Magnetic and EPR Measurements

Temperature-dependent magnetic susceptibility measurements on polycrystalline samples of **1** and **2** were made using a Quantum Design MPMS-XL-5 SQUID magnetometer over a temperature range of 1.8 to 300 K at a measuring field of 0.02 T. Magnetization measurements at variable temperature and variable field (VTVH) were performed at 1, 3, and 5 T over the temperature range of 1.8 to 300 K. A diamagnetic correction of 4.585 x 10^{-4} emu/mol for **1** and 5.139 x 10^{-4} emu/mol for **2** was calculated using Pascal constants[21] and was applied to the experimental data along with a contribution from the gelatin sample holder and straw. The magnetic properties were evaluated using the following standard spin Hamiltonian of a system with $S = {}^5/_2$ and zero-field splitting (zfs) terms, D and E.

$$\widehat{H} = \beta\vec{H}\cdot\tilde{g}\cdot\hat{S} + D\left(\hat{S}_z{}^2 - \widehat{\boldsymbol{S}}^2/3\right) + E\left(\hat{S}_x{}^2 - \hat{S}_y{}^2\right) \qquad (1)$$

In this Hamiltonian, β is the Bohr-magneton, $\vec{H}$ is the magnetic field vector, $\tilde{g}$ is the Zeeman tensor, *D* and *E* are the axial and rhombic zfs parameters, respectively, and the $\hat{S}$ terms are spin operators.[22] Since magnetic susceptibility measurements are typically insensitive towards the small energy of E, evaluation of both compounds began with the assumption of axial symmetry, thus E was assumed to be zero. Simulation of the experimental magnetic data was performed with the *julX* program.[23] It was necessary to include a small temperature-independent paramagnetism (*TIP*) term in the simulations according to $\chi_{calc} = \chi + TIP$.

Room temperature electron paramagnetic resonance (EPR) spectra were recorded on a Bruker E500 spectrometer equipped with X and Q-band microwave sources (9.4 and 34.5 GHz, respectively). The frequency was recorded with a built-in digital frequency counter and the magnetic field was calibrated using a 2,2-diphenyl-1-picrylhydrazyl standard (DPPH, g = 2.0036).[23] All samples were measured in quartz tubes that were sealed with approximately 1 inch of N-grease and lids. Signals from the instrument cavity and quartz tubes (Supporting Information Figure S1) were measured separately and were subtracted from the spectra of our samples. The spectra were analyzed by visual comparison with a locally developed computer simulation program, as described elsewhere.[24, 25]

2.3 Electrochemistry and Spectroelectrochemistry

Cyclic voltammograms were recorded using a BAS CV-50W Voltammetric Analyzer equipped with a three-electrode cell (3 mm Pt disk working electrode, Pt wire auxiliary electrode and a Ag/AgCl or Ag wire quasi-reference electrode) as described previously.[26] Solutions were 1 mM in analyte and 0.1 M in $[NBu_4]PF_6$ in CH_2Cl_2. Ferrocene (Fc) was used as an internal reference standard, with potentials (V) reported relative to the Fc/Fc^+ couple.[27]

IR spectroelectrochemical measurements were recorded using a Bruker Vector 22 FT-IR spectrometer equipped with a *Remspec* mid-IR fiber-optic dip probe and a liquid nitrogen cooled MCT detector. In our adaptation of the probe for these measurements,[28] the stainless steel mirror on the liquid transmission head of the fiber-optic dip probe was replaced with a 3 mm Pt disk working electrode and equipped with a custom-made electrochemical cell including a Pt wire auxiliary electrode and a Ag/AgCl or Ag wire quasi-reference electrode as described previously.[26, 29]

2.4 X-ray Crystallography

Intensity data for the crystals at 100(2) K were collected using a diffractometer with a Bruker APEX CCD area detector[30, 31] and graphite-monochromated Mo Kα radiation (λ = 0.71073 Å). A summary of the crystal and refinement data is shown in Table S1. The X-ray crystal structural data have been deposited with the Cambridge Crystallographic Data Center, with reference codes CCDC 1040731 (compound **1**), CCDC 1040732 (compound **2**), and CCDC 1040734 (compound **6**). These data can be obtained free of charge via www.ccdc.cam.ac.uk/ data_request/cif, by emailing data_request@ccdc.cam.ac.uk, or by contacting The Cambridge Crystallographic Data Center, 12 Union Road, Cambridge CB2 1EZ, UK; Fax: +44 1223 336033.

3 Results and Discussion

Synthesis

We are interested in the reactions of NO donors such as the general class of NONOate compounds with iron porphyrins as possible models for the interactions of these NONOates with various heme active sites. We previously reported the preparation of the *aryl* NONOate Cupferron iron porphyrin complexes (por)Fe(η^2-ON(Ph)NO) (por = TPP, T(*p*-OMe)PP) from the reactions of the (por)FeCl precursors with Ag[ON(Ph)NO].[11] We have now employed a more convenient route to prepare the hitherto unknown *alkyl* NONOate complexes (por)Fe(η^2-ON(*t*-Bu)NO) (por = OEP, TPP) using the readily obtainable porphyrin oxo-dimer precusors and *N*-*t*-butyl-*N*-nitrosohydroxylamine as shown in eq. 2. The analytically pure products were obtained in reasonable yields. The solids appear to be stable in air for short periods, but their solutions are sensitive to air as judged by IR spectroscopy. The IR spectrum of **1** as a KBr pellet reveals, in addition to the porphyrin bands, a new strong band at 1166 cm^{-1} associated with the N_2O_2

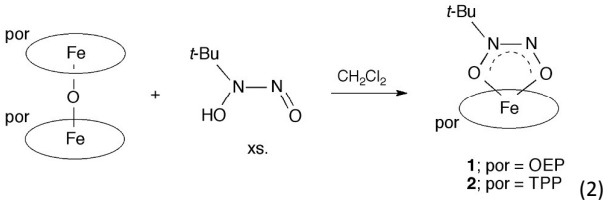

(2)

moiety.[32, 33] For compound **2**, in addition to the new related band at 1163 cm^{-1}, a new medium intensity band at 961 cm^{-1} is observed that is in a region associated with δ(ONNO).[32, 34] Other IR bands of the bidentate ligand are not readily discernable, presumably due to overlap with the porphyrin bands.

3.2 Molecular Structures

The crystal structures of **1** and **2**, the latter crystallizing as a CH_2Cl_2 solvate, are shown in Figure 2, with

(a)

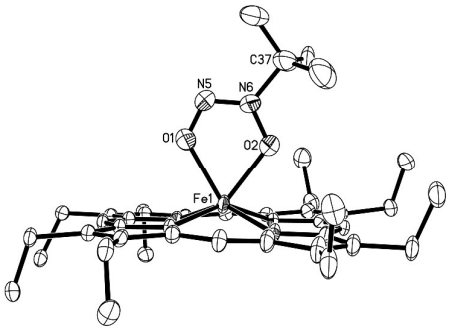

(b)

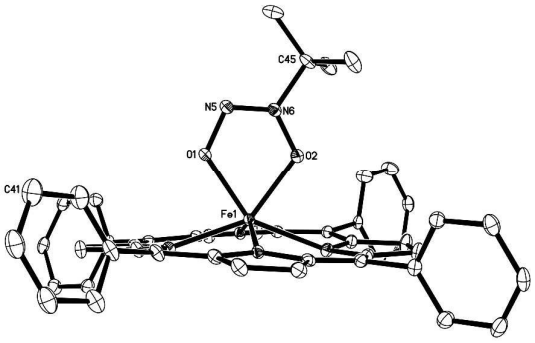

Fig. 2 Molecular structure of (a) (OEP)Fe(η^2-ON(*t*-Bu)NO) (**1**) (only the major disordered ligand (67% occupancy) orientation for **1** is shown), and (b) (TPP)Fe(η^2-ON(*t*-Bu)NO) (**2**). One of the porphyrin phenyl rings (with the C41 atom) is disordered; only the major component (85% occupancy) is shown. H atoms have been omitted for clarity. Thermal ellipsoids are drawn at 35%.

selected bond lengths and angles collected in Table 1. The most striking features of the structures are the bidendate *O,O*-binding modes of the ligand to the porphyrin Fe centers resulting in substantial apical Fe displacements (ΔFe) of +0.60 Å (for **1**) and

Table 1. Selected bond lengths (Å), bond angles (°) for **1** and **2**•(CH_2Cl_2).

	1	**2**•(CH_2Cl_2)
Fe–O1	2.118(5) [2.116(5)][a]	2.051(2)
Fe–O2	2.113(6) [2.114(6)][a]	2.050(2)
O1–N5	1.231(7) [1.232(8)][a]	1.306(3)
O2–N6	1.340(9) [1.342(9)][a]	1.313(3)
N5–N6	1.250(8) [1.252(9)][a]	1.261(4)
N6–C(CMe_3)	1.529(9)	1.495(4)
Fe–N(por)	2.073(4) – 2.104(4)	2.085(3) – 2.144(3)
∠O2–Fe–O1	68.0(3) [69.9(6)][a]	72.31(9)
∠N5–O1–Fe	122.3(8) [120.3(14)][a]	120.0(2)
∠N6–O2–Fe	113.6(5) [111.2(8)][a]	115.0(2)
∠N6–N5–O1	112.3(10) [113.6(19)][a]	111.8(3)
∠N5–N6–O2	118.6(8) [118.8(13)][a]	120.8(3)
∠N5–N6–C(CMe_3)	125.3(7) [128.8(12)][a]	121.4(3)
∠O2–N6–C(CMe_3)	114.6(6) [110.5(8)][a]	117.7(3)

[a] The data in brackets are for the disordered (second) component.

+0.69 Å (for **2**) from the 24-atom porphyrin planes towards the ligands. The Fe–O bond lengths are near equivalent at ~2.11 Å for **1** and ~2.05 Å for **2**, with respective O–Fe–O bite angles of 68.0(3)° (with 69.9(6)° for the minor component) for compound **1** and 72.3(1)° for compound **2**. It is interesting to note that for the OEP derivative **1**, the terminal N5–O1 bond length of 1.231(7) Å (1.232(8) Å for minor component) is significantly shorter than the N6-O2 bond length (1.340(9) Å), whereas the related N–O bond lengths in the TPP derivative are closer to each other (1.306(3) and 1.313(3) Å, respectively). The ONNO moiety in **2** (ONNO torsion angle of 0.6(4)°) is nearly planar, compared with the wider torsion angle of 9.2(15)° (–19(3)° for the minor component) of compound **1**, although both compounds possess N6 atoms with essentially planar geometries. The N–N bond length of **1** is 1.250(8) Å, and is 1.261(4) Å in **2**.

The η^2-*O,O* binding mode of the axial ligands in **1**, **2**, and **4** is uncommon;[35, 36] there are only three other iron porphyrin complexes that display this η^2-*O,O* binding mode, namely the high-spin ferric nitrato complexes (TPP)Fe(NO_3)[37] and (TpivPP)Fe(NO_3),[38, 39] and the ferric tropolonate complex (OEP)Fe($O_2C_7H_5$)[40] (Table 2).

Table 2. Structural data for η^2-*O,O* liganded iron(III) porphyrins.

	Fe-O (Å)	O-Fe-O (°)	ΔFe (Å)[b]
1[a]	2.113(6) 2.118(5)	68.0(3)	0.60
2	2.051(2) 2.050(2)	72.31(9)	0.69
4	2.044(3) 2.091(2)	71.52(9)	0.69
(TPP)Fe(NO_3)	2.019(4) 2.323(8)	51.6(2)	0.60
(TpivPP)Fe(NO_3)	2.123(3) 2.226(3)	57.75(10	0.61
(OEP)Fe($O_2C_7H_5$)	2.064(6) 2.067(6)	73.1(2)	0.80

[a] For the major disordered component. [b] apical displacement from the 24-atom porphyrin planes.

The X-ray crystal structural data for **1** and **2** are indicative of these high-spin ferric complexes, using the stereochemical/spin-state relationships described by Scheidt and Reed.[41] To probe possible changes in spin-states and associated spin-crossover[42, 43] temperatures of complexes **1** and **2**, we embarked on detailed variable-temperature magnetic studies of these complexes.

3.3 Magnetic Behavior

Magnetic susceptibility (χ) measurements were undertaken to establish the electronic spins of **1** (por = OEP) and **2** (por = TPP). The magnetic moments of **1** and **2** were found to be 5.976 μ_B and 5.974 μ_B, respectively at room temperature, that is, close to the spin-only value for an $S = {}^5/_2$ system (5.916 μ_B for g = 2). The magnetic moments of both compounds remain nearly constant down to 20 K, but decrease sharply below 20 K, as shown in Figure 4. The sharp decrease in μ_{eff} suggested that both compounds have significant zero-field splitting (zfs) resulting from spin-spin and spin-orbit coupling, as expected for an S = ${}^5/_2$ state in noncubic environment.[44]

The data in Figure 3 were well simulated using the parameters $S = {}^5/_2$, D = 4.3 ± 0.2 cm^{-1}, and g_{avg} = 2.02 ± 0.01. Further confirmation of these parameters was achieved by variable temperature/variable field (VTVH) magnetization measurements (1.8–300 K). The VTVH data for both compounds are shown in the inset of Figure 3. These data were well simulated using $S = {}^5/_2$, g_{avg} = 2.02 ± 0.01 and D = 3.6 ± 0.2 cm^{-1}, which is in good agreement with the susceptibility results. In both compounds the magnetic data are consistent with the assignment of an $S = {}^5/_2$ high-spin (HS) ferric (Fe^{3+}) ion. Since magnetization and magnetic susceptibility are not the most accurate methods for determining *D* or *g*, a detailed EPR study was undertaken.

Figure 4 shows the room temperature, X-band (9.4 GHz) powder EPR spectra of both compounds (middle segment, blue (compound **1**) and black (compound **2**)). Also shown are the simulated energy level diagrams with the magnetic field orientation parallel to the principal symmetry axis of the molecule (H || z) and parallel to the *x*, *y* directions (top and bottom segments respectively). The simulated energy level diagrams and EPR spectra

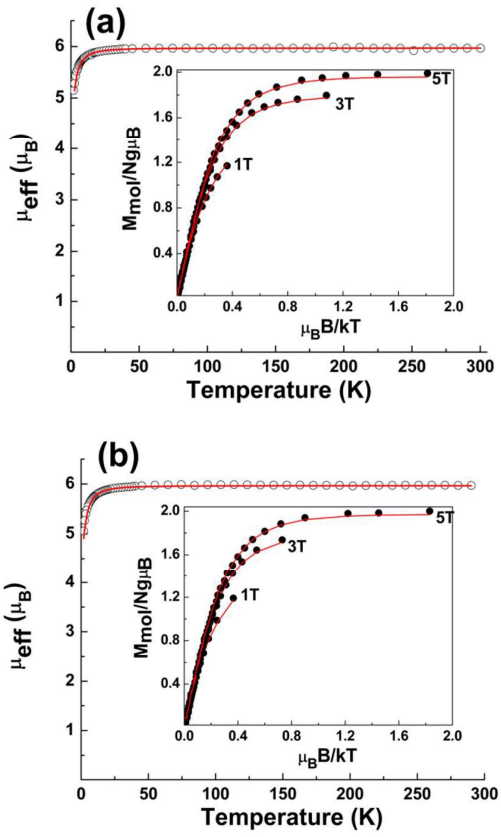

Fig. 3 Temperature dependence of μ_{eff} (main figure) and VTVH measurements (inset) for compounds **1** and **2** labeled (a) and (b) respectively. The solid lines represent the best fit simulations to the experimental data using S = $^5/_2$, g_{avg} = 2.02 ± 0.01, and D = 4.3 ± 0.2 $cm^{-1}$for μ_{eff} , and $S = {}^5/_2$, g_{avg} = 2.02 ± 0.01 and D = 3.6 ± 0.2 cm^{-1} for VTVH measurements.

were calculated using a locally developed computer program,[45, 46] which diagonalizes the Hamiltonian matrix of equation 1.

At X-band (9.4 GHz), two distinct features were seen, at g' = 7.60 and g' = 4.15. Computer simulations of the X-band spectra (middle segment, red trace), using the parameters: $S = {}^5/_2$, g_z =2.03 ± 0.03 , $g_{x,y}$ =1.97 ± 0.03, $|D|$ = 3.89 cm^{-1} ± 0.09, and E/D = 0.07 ± 0.01, are in good agreement with the experimental spectra with minor artifacts due to an imperfectly random distribution of crystallites in the used powder sample, not an uncommon feature in powder EPR studies. The EPR peaks are rather broad, thus suggesting g-anisotropy due to the electrostatic field from neighboring porphyrin molecules. Similarly broadened spectra have been previously reported for ferric nitrato porphyrinates.[39] A small, sharp peak was observed at g = 2.02, which is tentatively ascribed to a minor S = ½ impurity or decomposed product (see Supporting Information).

X-band analysis is confirmed by additional measurements at Q-band (34.5 GHz), a four-fold higher microwave frequency. The improved resolution provided by Q-band (34.5 GHz), splits the spectra into three peaks at g' = 7.59, 5.58, and 4.15 as shown in

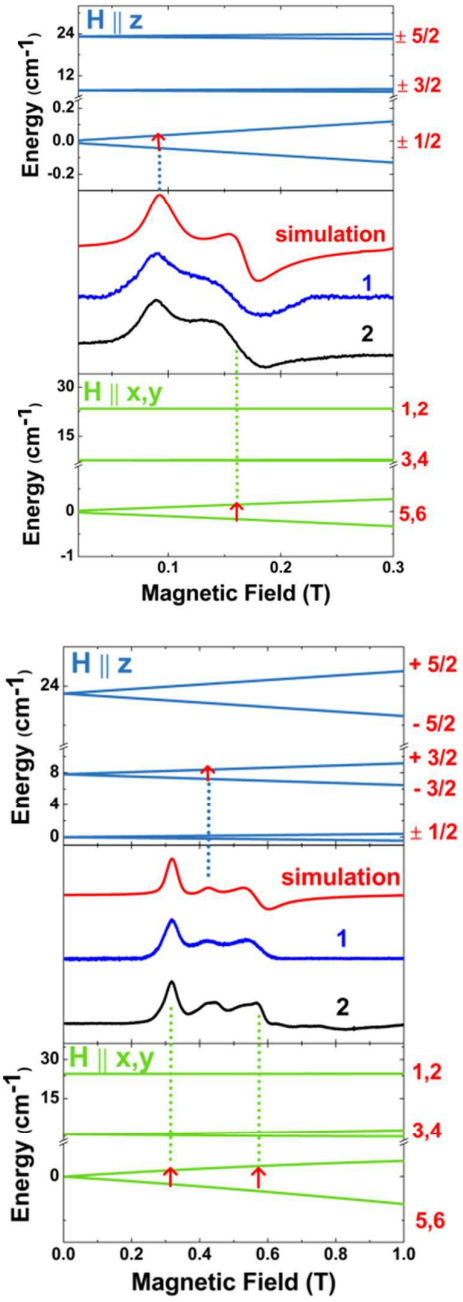

Fig. 4 ***Top***: X-band (9.4 GHz) EPR experimental and simulation spectra of **1** (por = OEP) and **2** (por = TPP) at room temperature. ***Botom*** Q-band (34.5 GHz) EPR experimental and simulation spectra of **1** and **2**. The top and bottom portions in each figure show the energy level diagrams, for the H || z and H || x, y directions respectively. The red numbers in the top figure represent the M_s quantum numbers in the high-field limit. In the bottom figure; however, they are just labels for energy levels since the field strength was not enough to be in the ' high-field' limit. Red arrows mark the EPR transition assignment.

Figure 4 (middle segment). The Q-band spectra were well fit using the same parameters as the X-band data. At both frequencies we label the g values with prime symbols indicating that they are only

effective values, which are skewed from the usual high-spin Fe^{3+} values (g ~2.002–2.009),[22, 47-49] due to large zfs, a result that has been seen in many high-spin Fe^{3+} systems.[22, 47-49] For example, the report of large g-values has been seen in biological systems with high spin ferric ions like the heme proteins[47-51] and in other Fe^{3+} porphyrinates where the effective g values have been shown to range from ~7.7 to 1.8.(ref 40).

The EPR data, combined with magnetic susceptibility, unambiguously show that the iron center in these compounds exists as a high-spin ferric ion, with a large axial zfs and non vanishing rhombic zfs.

3.4 Redox Behavior and IR Spectroelectrochemistry

The redox behavior of compounds **1** and **2** in CH_2Cl_2 was investigated by cyclic voltammetry and infrared spectroelectrochemistry. The cyclic voltammagrams are shown in Figure 5. Both compounds **1** and **2** show well-defined reverisble first oxidations. The OEP derivative **1** is oxidized at an $E^{o'}$ potential of +0.27 V versus the Fc/Fc^+ couple, lower than that of the TPP analog that displays its redox couple at +0.44 V. The difference in the magnitude of redox couples is reflective of the influence of the electron-donating capacity of the macrocycles (OEP > TPP),[52] suggestive of electrooxidations at a site in close proximity to or on the porphyrin macrocycles (*vide infra*).

The OEP derivative **1** displays an irreversible reduction with E_{pc} at −1.60 V and an associated small return peak at −0.99 V. In contrast, the TPP analogue **2** exhibits a reversible reduction couple with $E^{o'}$ at −1.26 V. The peak separation of this reduction couple (0.33 V) is larger than that of the Fc/Fc^+ couple (0.14 V) under identical conditions, indicative of a quasi-reversible reduction and/or slow electron transfer during the reduction process.

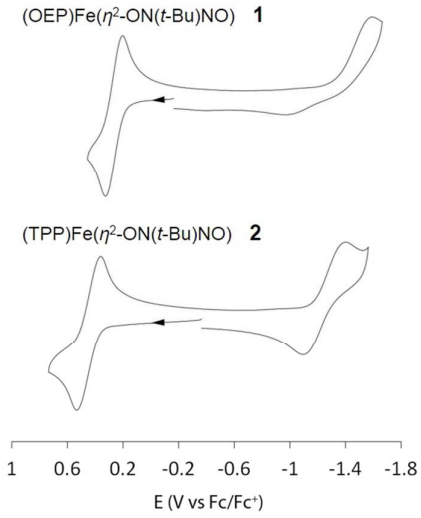

Fig. 5 Cyclic voltammograms of the (por)Fe(η^2-ON(*t*-Bu)NO) (por = OEP, TPP) compounds in CH_2Cl_2 containing 0.1 M NBu_4PF_6 and at a scan rate of 0.2 V/s at room temperature.

IR spectroelectrochemistry of compound **1** upon oxidation was investigated under the same experimental conditions used for the cyclic voltammetry experiments, with the applied potential held slightly above the E_{pa} for the first oxidation. The resulting difference IR spectrum is shown in Figure 6. Importantly, an intense new band at 1541 cm^{-1} grew in after the first oxidation; this band is in the region associated with the characteristic bands for OEP containing π-radical monocations.[20] No new band was detected in the range typical for ferric-NO moieties.[14]

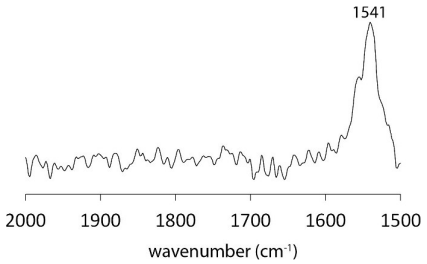

Fig. 6 Difference FTIR (spectrum) showing formation of the porphyrin radical product during the first oxidation of (OEP)Fe(η^2-ON(*t*-Bu)NO).

Based on both the cyclic voltammetry and spectroelectrochemistry results, we conclude that the bound diazeniumdiolate ligand is retained upon oxidation, and that the oxidation occurs on the macrocycle and not on the axial metal-ligand fragment (eq. 3).

$$(por)Fe(\eta^2\text{-}ON(t\text{-}Bu)NO) \rightarrow (por^{\bullet+})Fe(\eta^2\text{-}ON(t\text{-}Bu)NO) + e^- \quad (3)$$

The difference IR spectrum obtained during spectroelectrochemical oxidation of **2** does not show any new band formed in the 2000–1500 cm^{-1} region. We note that the characteristic bands of tetraarylporphyrin radicals at 1295–1270 cm^{-1} in the IR spectra[20] are outside of the accessible IR spectral window of our instrumentation. However, chemical oxidation of (TPP)Fe(η^2-ON(*t*-Bu)NO) using $AgBF_4$ (see Experimental Section) results in a product with a new band at 1293 cm^{-1}, consistent with the generation of the $(TPP^{\bullet+})$Fe(η^2-ON(*t*-Bu)NO) radical cation product as described in eq. 6.

3.5 Reactivity

The final products obtained when (OEP)Fe(η^2-ON(*t*-Bu)NO) was reacted with 1-MeIm were not the expected six-coordinate compounds shown in eq. 4, but rather the known nitrosyl compound (OEP)Fe(NO) (υ_{NO} = 1665 cm^{-1}) and the organic *t*-BuNO product, the latter characterized by ^1H NMR spectroscopy. No stable six-coordinate product was obtained in this case.

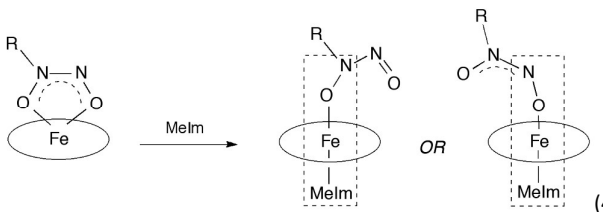

(4)

We propose that the reaction of eq. 4 results in the elimination of both NO and *t*-BuNO, with NO being the only reagent capable of re-binding to Fe, as the *t*-BuNO ligand is likely too bulky to re-bind effectively with the Fe porphyrin.

Indeed, to examine this proposed reaction pathway further, we prepared the related Cupferron analog (OEP)Fe(η^2-ON(Ph)NO) (**3**) and performed a similar reaction with 1-MeIm. In this case, we were successful at isolating both the known five-coordinate (OEP)Fe(NO) compound and the six-coordinate derivative (OEP)Fe(PhNO)(1-MeIm) that we identified by IR spectroscopy and X-ray crystallography.[16] The analogous reaction of (T(*p*-OMe)PP)Fe(η^2-ON(Ph)NO) (**4**) with 1-MeIm generated the nitrosyl

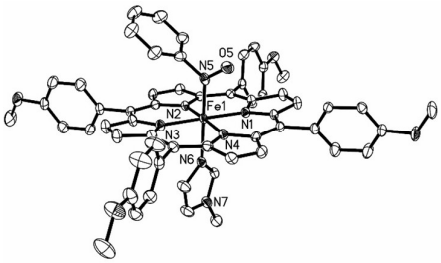

Fig. 7. Molecular structure of (T(*p*-OMe)PP)Fe(PhNO)(1-MeIm) (**6**). H atoms have been omitted for clarity. Thermal ellipsoids are drawn at 50%. Selected bond lengths and angles: Fe1–N5 = 1.795(2) Å, Fe1–N6 = 2.044(2) Å, Fe1–N5–O5 = 123.4(2)°, N5–Fe1–N6 = 178.8(1)°, N4–Fe1–N5–O5 = 38.1(2)°.

compound (T(*p*-OMe)PP)Fe(NO) and the new six-coordinate (T(*p*-OMe)PP)Fe(PhNO)(1-MeIm) (**6**) derivative that were characterized by IR spectroscopy and X-ray crystallography (Figure 7).

The C-N-O plane of the PhNO ligand bisects adjacent porphyrin N atoms, and the axial ligands are essentially mutually perpendicular. Similar axial ligand orientations have been observed previously for (OEP)Fe(*i*-PrNO)(py),[53] (por)Fe(*i*-PrNO)(1-MeIm) (por = TPP, TTP),[53] and (TPP)Fe(PhNO)$_2$,[54] although parallel (or near-parallel) orientations are present in the crystal structures of (OEP)Fe(*i*-PrNO)(1-MeIm),[53] and related complexes.[16]

Based on the products formed from the reactions of the NONOate compounds with 1-MeIm (top of Scheme 1; path A), we propose the initial binding of 1-MeIm *trans* to the NONOate group would likely need to be coincident with a bidentate-to-monodentate binding shift of the NONOate group, analogous to the products of eq. 4. Surprisingly, there is only a single structural precedent for such a monodentate NONOate binding (in a Cu complex).[7] Decomposition of this (1-MeIm)Fe(η^1-ON(R)NO) intermediate then results in the release of RNO and Fe-bound NO. We note that we obtained the (por)Fe(RNO)(1-MeIm) and (por)Fe(NO) products in relatively low yields (~50% total isolated yield based on Fe) and were not successful in identifying the other products of the reaction, hence this proposed path for the reaction with 1-MeIm is likely not the complete picture for this reaction pathway.

We also explored a possible adduct formation between the (por)Fe(η^2-ON(*t*-Bu)NO) compounds and NO to generate the six-coordinate (por)Fe(NO)(η^1-ON(*t*-Bu)NO) products. Addition of NO

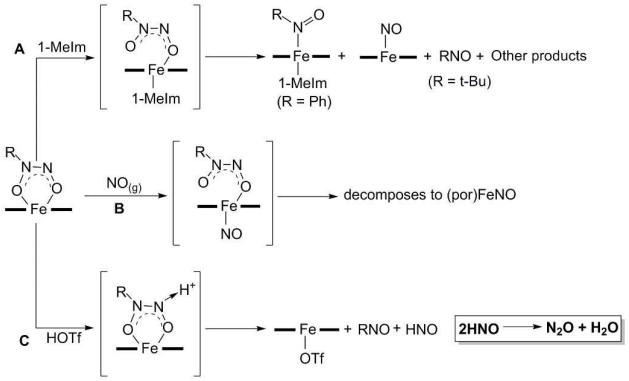

Scheme 1. Proposed reaction pathways of (por)Fe(η^2-ON(R)NO). (A) Reaction with 1-MeIm, (B) Reaction with NO, (C) Protonation reaction with triflic acid (HOTf).

(or ^{15}NO) to **1** in CH_2Cl_2 yielded a product with a υ_{NO} band at 1883 cm^{-1} (υ_{15NO} 1848 cm^{-1}) assigned to the desired nitrosyl (OEP)Fe(NO)(η^1-ON(*t*-Bu)NO) product (Scheme 1; path B). The related nitrosyl (TPP)Fe(NO)(η^1-ON(*t*-Bu)NO) product displayed its υ_{NO} at 1888 cm^{-1} (υ_{15NO} 1851 cm^{-1}). Although there are no isolable (por)Fe(NO)(alkoxide) compounds reported in the literature, the υ_{NO} of (TPP)Fe(NO)(η^1-ON(*t*-Bu)NO) at 1888 cm^{-1} is lower than the υ_{NO} of the neutral nitrosyl trifluroacetate compound (TPP)Fe(NO)(OC(=O)CF$_3$) at 1907 cm^{-1}.[55] Unfortunately, all attempts to isolate the (por)Fe(NO)(η^1-ON(*t*-Bu)NO) products from solution resulted in their decomposition to the known five-coordinate (por)Fe(NO) derivatives.

Another important biologically-relevant reaction that we examined was the protonation of the (por)Fe(η^2-ON(R)NO) complexes. Similar to the reactions with 1-MeIm described above, these protonation reactions were performed under reduced laboratory lighting to minimize the light-induced decomposition of the starting (por)Fe(η^2-ON(R)NO) compounds. Reaction of (OEP)Fe(η^2-ON(*t*-Bu)NO) (**1**) with anhydrous triflic acid generated the known (OEP)Fe(OTf) that was characterized by X-ray crystallography, with *t*-BuNO as the organic product that was identified by ^{1}H NMR spectroscopy (path C in Scheme 1). Interestingly, gas-phase IR spectroscopic analysis of the collected headspace gases revealed the formation of N_2O. The analogous protonation reaction with the Cupferron complex (T(*p*-OMe)PP)Fe(η^2-ON(Ph)NO) (**4**) likewise yielded N_2O gas as a product.

Based on these results, we propose that protonation likely occurs at the "exposed" N5 atoms, as both O-atoms of the NONOate group are involved in binding to the ferric center in the (por)Fe(η^2-ON(R)NO) complexes (i.e., pathway C in Scheme 1).

Similar *N*-protonations have been considered in the pH-dependent decompositions of NONOates to help explain the release of HNO in these systems.[56, 57] This protonated [(por)Fe(η^2-ON(R)N(H)O)]$^+$ intermediate would then release both RNO and HNO, the latter decomposing according to its known dimerization[58, 59] to the observed N_2O gas.

4 Conclusions

This report shows that the alkyl NONOates **1** and **2** are isolable and characterizable by X-ray structural, spectroelectrochemical and magnetic measurements. These species may thus be more stable than previously thought. The detailed magnetic studies showing high-spin ($S = {}^{5}/_{2}$) formulations for these ferric compounds are consistent with the significant apical displacements of the Fe centers towards the axial *O,O*-bidentate ligands. Although **1** and **2** are thermodynamically stable, they are reactive towards a histidine mimic (1-MeIm), NO, and protons, shedding additional insight into *C*-NONOate decomposition pathways in the presence of metals.

Acknowledgements

We are grateful to the National Science Foundation (CHE-1213674 to GBR-A) for funding for this work. J.H.C. and N.S.D. wish to thank Catherine Kent and Tiffany Brooks for valuable assistance with the magnetic measurements.

Supporting Information

Tables of X-ray crystallography data and figures for the crystal structures of **1**, **2**, and **6**. Figures for the X-band and Q-band empty cavity and quartz tube profiles, Boltzmann populations and full Q and X-band EPR spectra for **1** and **2**.

References

1. J. A. Hrabie and L. K. Keefer, *Chem. Rev.,* 2002, **102**, 1135-1154.
2. R. C. Mehrotra in *Hydroxamates, Cupferron and Related Ligands*, *Vol. 2* (Ed. G. Wilkinson), Pergamon Press, U. K., **1987**, pp. 505-514 (Chapter 15.9).
3. H. N. Jayaram, A. K. Tyagi, S. Anandaraj, J. A. Montgomery, J. A. Kelley, J. Kelley, R. H. Adamson and D. A. Cooney, *Biochem. Pharmacol.,* 1979, **28**, 3551-3566.
4. Y. K. S. Murthy, J. E. Thiemann, Coronell.C and P. Sensi, *Nature,* 1966, **211**, 1198-1199.
5. T. Natori, Y. Kataoka, S. Kato, H. Kawai and N. Fusetani, *Tetrahedron Letters,* 1997, **38**, 8349-8350.
6. P. G. Wang, M. Xian, X. Tang, X. Wu, Z. Wen, T. Cai and A. J. Janczuk, *Chem. Rev.,* 2002, **102**, 1091-1134.
7. J. L. Schneider, J. A. Halfen, V. G. Young and W. B. Tolman, *New J. Chem.,* 1998, **22**, 459-466.
8. T. A. Alston, D. J. T. Porter and H. J. Bright, *J. Biol. Chem.,* 1985, **260**, 4069-4074.
9. H. A. Hassanin, L. Hannibal, D. W. Jacobsen, M. F. El-Shahat, M. S. A. Hamza and N. E. Brasch, *Angew. Chem. Int. Ed.,* 2009, **48**, 8909-8913.
10. M. Shiino, Y. Watanabe and K. Umezawa, *Bioorg. Med. Chem.,* 2001, **9**, 1233-1240.
11. G.-B. Yi, M. A. Khan and G. B. Richter-Addo, *Inorg. Chem.,* 1995, **34**, 5703-5704.
12. N. Arulsamy, D. S. Bohle, J. A. Imonigie and E. S. Sagan, *J. Am. Chem. Soc.,* 2000, **122**, 5539-5549.
13. M. Ahmed, A. J. Edwards, C. J. Jones, J. A. McCleverty, A. S. Rothin and J. P. Tate, *J. Chem. Soc., Dalton Trans.,* 1988, 257-263.
14. L. Cheng and G. B. Richter-Addo in *The Porphyrin Handbook*, Vol. 4; R. Guilard, K. Smith and K. M. Kadish, Eds.; Academic Press, New York, **2000**, pp 219-291.
15. J. P. Freeman, *J. Org. Chem.,* 1963, **28**, 2508-2511.
16. N. Godbout, L. K. Sanders, R. Salzmann, R. H. Havlin, M. Wojdelski and E. Oldfield, *J. Am. Chem. Soc.,* 1999, **121**, 3829-3844.
17. A. Lapinski, J. Spanget-Larsen, J. Waluk and J. G. Radziszewski, *J. Chem. Phys.,* 2001, **115**, 1757-1764.
18. H. E. Gottlieb, V. Kotlyar and A. Nudelman, *Journal of Organic Chemistry,* 1997, **62**, 7512-7515.
19. J. A. Gonzalez and L. J. Wilson, *Inorg. Chem.,* 1994, **33**, 1543-1553.
20. E. T. Shimomura, M. A. Phillippi, H. M. Goff, W. F. Scholz and C. A. Reed, *J. Am. Chem. Soc.,* 1981, **103**, 6778-6780.
21. G. A. Bain and J. F. Berry, *J. Chem. Educ.,* 2008, **85**, 532-536.
22. R. Boča, *Coord. Chem. Rev.,* 2004, **248**, 757-815.
23. J. Krzystek, A. Sienkiewicz, L. Pardi and L. C. Brunel, *J. Magn. Reson.,* 1997, **125**, 207-211.
24. P. P. Samuel, K. C. Mondal, N. A. Sk, H. W. Roesky, E. Carl, R. Neufeld, D. Stalke, S. Demeshko, F. Meyer, L. Ungur, L. F. Chibotaru, J. Christian, V. Ramachandran, J. van Tol and N. S. Dalal, *J. Am. Chem. Soc.,* 2014, **136**, 11964-11971.
25. W. J. Liu, J. H. Christian, R. Al-Oweini, B. S. Bassil, J. van Tol, M. Atanasov, F. Neese, N. S. Dalal and U. Kortz, *Inorg. Chem.,* 2014, **53**, 9274-9283.
26. Z. N. Zahran, M. J. Shaw, M. A. Khan and G. B. Richter-Addo, *Inorg. Chem.,* 2006, **45**, 2661-2668.
27. N. G. Connelly and W. E. Geiger, *Chem. Rev.,* 1996, **96**, 877-910.
28. M. J. Shaw, R. L. Henson, S. E. Houk, J. W. Westhoff, M. W. Jones and G. B. Richter-Addo, *J. Electroanal. Chem.,* 2002, **534**, 47-53.
29. S. M. Carter, J. Lee, C. A. Hixson, D. R. Powell, R. A. Wheeler, M. J. Shaw and G. B. Richter-Addo, *Dalton Trans.,* 2006, 1338-1346.
30. *APEX2 Software Reference Manual*, Bruker-AXS, Madison, WI, **2007**.
31. *Data Reduction: SAINT Software Refence Manual.* Bruker-AXS, Madison, WI. *,* 2007.
32. I. J. Casely, Y. Suh, J. W. Ziller and W. J. Evans, *Organometallics,* 2010, **29**, 5209-5214.
33. L. K. Keefer, J. L. Flippen-Anderson, C. George, A. P. Shanklin, T. A. Dunams, D. Christodoulou, J. E. Saavedra, E. S. Sagan and D. S. Bohle, *Nitric Oxide: Biol. Chem.,* 2001, **5**, 377-394.
34. A. Deak, I. Haiduc, L. Parkanyi, M. Venter and A. Kalman, *Eur. J. Inorg. Chem.,* 1999, 1593-1596.
35. W. R. Scheidt, *J. Porph. Phthalocyanines,* 2008, **12**, 979-992.
36. W. R. Scheidt in *The Porphyrin Handbook*, *Vol. 3*; K. M. Kadish, K. M. Smith and R. Guilard, Eds.: Academic Press, New York, **2000**, Chapter 16, pp 49-112.
37. M. A. Phillippi, N. Baenziger and H. M. Goff, *Inorg. Chem.,* 1981, **20**, 3904-3911.
38. O. Q. Munro and W. R. Scheidt, *Inorg. Chem.,* 1998, **37**, 2308-2316.
39. G. R. A. Wyllie, O. Q. Munro, C. E. Schulz and W. R. Scheidt, *Polyhedron,* 2007, **26**, 4664-4672.
40. L. Cheng, M. A. Khan, D. R. Powell, R. W. Taylor and G. B. Richter-Addo, *Chem. Commun.,* 1999, 1941-1942.
41. W. R. Scheidt and C. A. Reed, *Chem. Rev.,* 1981, **81**, 543-555.
42. T. Ikeue, Y. Ohgo, O. Ongayi, M. G. H. Vicente and M. Nakamura, *Inorg. Chem.,* 2003, **42**, 5560-5571.

43. T. Ikeue, Y. Ohgo, T. Yamaguchi, M. Takahashi, M. Takeda and M. Nakamura, *Angew. Chem. Int. Ed.,* 2001, **40**, 2617-2620.
44. J. A. Weil and J. R. Bolton, *Electron Paramagnetic Resonance Elementary Theory and Practical Applications*, 2nd Ed.: Wiley-Interscience, Hoboken, NJ, **2007**.
45. J. Krzystek, S. A. Zvyagin, A. Ozarowski, S. Trofimenko and J. Telser, *J. Magn. Reson.,* 2006, **178**, 174-183.
46. J. Krzystek, A. Ozarowski and J. Telser, *Coord. Chem. Rev.,* 2006, **250**, 2308-2324.
47. V. V. Laguta, M. D. Glinchuk, I. P. Bykov, Y. L. Maksimenko, J. Rosa and L. Jastrabik, *Phys. Rev. B,* 1996, **54**, 12353-12360.
48. R. G. Pontin, E. F. Slade and D. J. E. Ingram, *J. Phys. C Solid State Phys.,* 1969, **2**, 1146-1150.
49. A. Priem, P. J. M. van Bentum, W. R. Hagen and E. J. Reijerse, *Appl. Magn. Reson.,* 2001, **21**, 535-548.
50. A. Abragam and B. Bleaney, *Electron Paramagnetic Resonance of Transition Ions*, Oxford Press, Oxford, **1970**, pp 430-433.
51. J. R. Pilbrow, *Transition Ion Electron Paramagnetic Resonance*, Clarendon Press, Oxford, **1990**.
52. K. M. Kadish, E. Van Caemelbecke and G. Royal in *The Porphyrin Handbook, Vol. 8*; K. M. Kadish, K. M. Smith and R. Guilard, Eds.: Academic Press, San Diego, CA, **2000**, Chapter 55.
53. C. D. Sohl, J. Lee, S. S. Alguindigue, M. A. Khan and G. B. Richter-Addo, *J. Inorg. Biochem.,* 2004, **98**, 1238-1246.
54. L.-S. Wang, L. Chen, M. A. Khan and G. B. Richter-Addo, *Chem. Commun.,* 1996, 323-324.
55. N. Xu, L. E. Goodrich, N. Lehnert, D. R. Powell and G. B. Richter-Addo, *Angew. Chem. Int. Ed. Engl.,* 2013, **52**, 3896-3900.
56. D. J. Salmon, C. L. T. de Holding, L. Thomas, K. V. Peterson, G. P. Goodman, J. E. Saayedra, A. Srinivasan, K. M. Davies, L. K. Keefer and K. M. Miranda, *Inorg. Chem.,* 2011, **50**, 3262-3270.
57. A. S. Dutton, C. P. Suhrada, K. M. Miranda, D. A. Wink, J. M. Fukuto and K. N. Houk, *Inorg. Chem.,* 2006, **45**, 2448-2456.
58. K. M. Miranda, *Coord. Chem. Rev.,* 2005, **249**, 433-455.
59. V. Shafirovich and S. V. Lymar, *J. Am. Chem. Soc.,* 2003, **125**, 6547-6552.

Table of Contents graphic